Electronic Supplementary Information

Determination of products

Determination of NO_3^--N:[1]

The collected electrolyte was diluted several times to the detection range. 100 μL of 1 M HCl solution and 10 μL of 0.8 wt% sulfamic acid solution were added to 5 mL of diluted electrolyte and mixed for 10 min. Then, the absorption spectrum of the mixed solution was recorded using ultraviolet-visible (UV-vis) spectrophotometry in the wavelength range of 300-200 nm. The absorbance value was corrected by the following equation: $A=A_{220nm}-2A_{275nm}$. A series of KNO_3 standard solutions were prepared to obtain the calibration curve.

Determination of NO_2^--N:[1]

To determine the concentration of NO_2^--N, the color reagent was first obtained through a mixed solution containing p-aminobenzenesulfonamide (0.4 g), N-(1-Naphthyl) ethylenediamine dihydrochloride (0.02 g), phosphoric acid (1 mL, ρ=1.70 g/mL) and deionized water (5 mL). Then, the color reagent (100 μL) and the diluted electrolyte (5 mL) were mixed for 20 min. Finally, the absorption spectrum of the mixed solution was recorded using UV-vis spectrophotometry in the wavelength range of 650-450 nm. A series of $NaNO_2$ standard solutions were prepared to obtain the calibration curve.

Determination of NH_3-N:[1]

Nessler's reagent was used to determine the ammonia concentration. First, to prepare Nessler's reagent, KI (17.5 g) and Hg_2I (25.0 g) were dissolved in 4.0 M KOH solution (250 mL) and stored in the dark for 24 h. Then, potassium sodium tartrate solution (0.1 mL, ρ=500 g/L) and Nessler's reagent (0.1 mL) were added to diluted electrolyte (5 mL). Finally, the absorption spectrum of NH_3-

N was recorded using UV-vis spectrophotometry in the wavelength range of 530-380 nm. The calibration curve was obtained by using a series of standard NH_4Cl solutions.

Isotope Labeling Experiments

$K^{15}NO_3$ (99%) was used as the feeding nitrogen source to perform the isotopic labeling experiments to clarify the source and quantify the concentration of ammonia-N. After electroreduction for 2 h in 0.5 M K_2SO_4 solution containing 50 mg L^{-1} $K^{15}NO_3$-^{15}N. The post-electrolysis electrolyte was collected and the pH value was adjusted to weak acid by 4 M H_2SO_4. The $^{15}NH_4^+$-^{15}N concentration was quantified by ^1H NMR with external standard of maleic acid ($C_4H_4O_4$). First, various amounts of $^{15}NH_4^+$-^{15}N (10, 20, 30, 40, 50 mg L^{-1}) were dissolved in 0.5 M K_2SO_4 with 50 mg L^{-1} $C_4H_4O_4$ as a standard solution. Then, 50 μL of deuterium oxide (D_2O) was mixed with 0.5 mL of the acidified electrolyte or standard solution to obtain further ^1H NMR spectra by the NMR detection.

Calculation of the conversion rate, yield, selectivity, and Faradaic efficiency

The calculation equation is as follows:

$$\text{Conversion} = \Delta c_{NO_3^-} / c_0 \times 100\% \quad (1)$$

$$\text{Yield}_{NH_3} = (c_{NH_3} \times V) / (M_{NH_3} \times t \times m) \quad (2)$$

$$\text{Selectivity}\ (NH_3) = c_{NH_3} / \Delta c_{NO_3^-} \times 100\% \quad (3)$$

$$\text{Selectivity}\ (NO_2^-) = c_{NO_2^-} / \Delta c_{NO_3^-} \times 100\% \quad (4)$$

$$\text{Faradaic efficiency} = (8F \times c_{NH_3} \times V) / (M_{NH_3} \times Q) \quad (5)$$

Where Δc_{NO3}^- is the concentration difference of NO_3^- before and after reduction, c_0 is the initial concentration of NO_3^-, c_{NH3} is the measured NH_3 concentration, V is the electrolyte volume in the cathode chamber (35 mL), t is the electrolysis time (2 h), M_{NH3} is the molar mass of NH_3, m is the catalyst mass (1 mg), c_{NO2}^- is the concentration of NO_2^-, F is the Faraday constant (96 485 C mol^{-1}), and Q is the total charge during electrolysis.

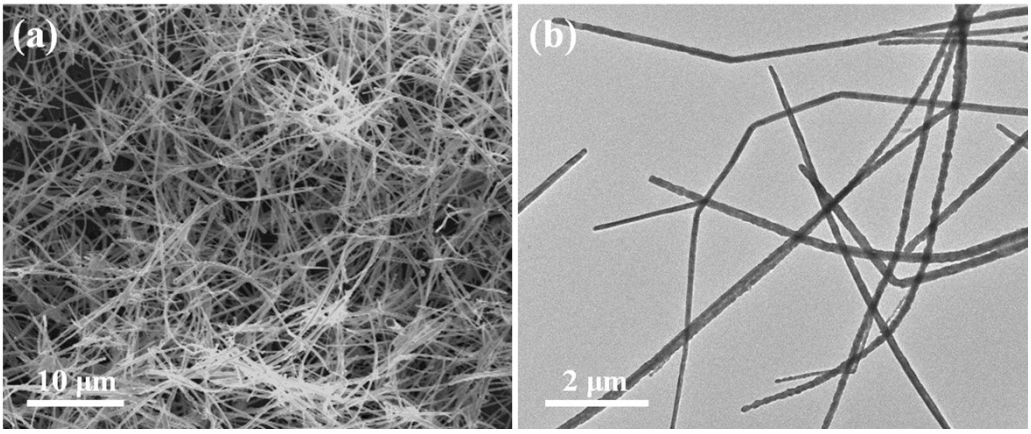

Fig. S1 SEM (a), and TEM (b) images of the Cu nanowires.

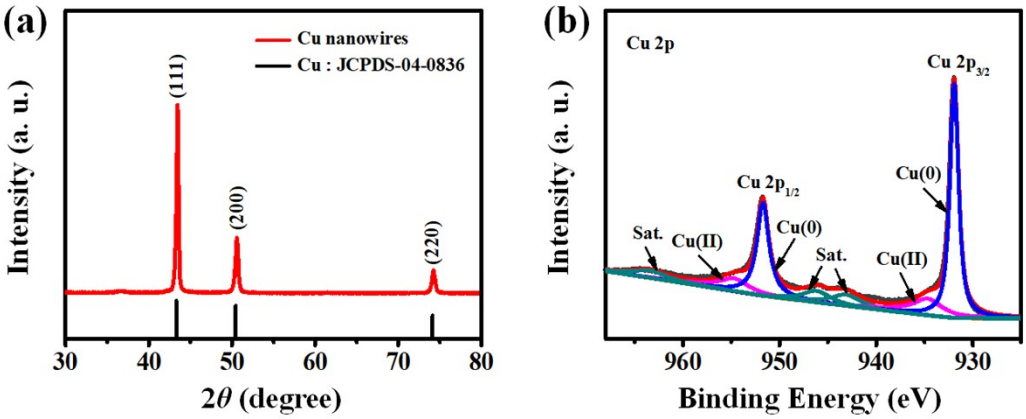

Fig. S2 XRD pattern (a), and high-resolution XPS spectrum of Cu 2p (b) for Cu nanowires.

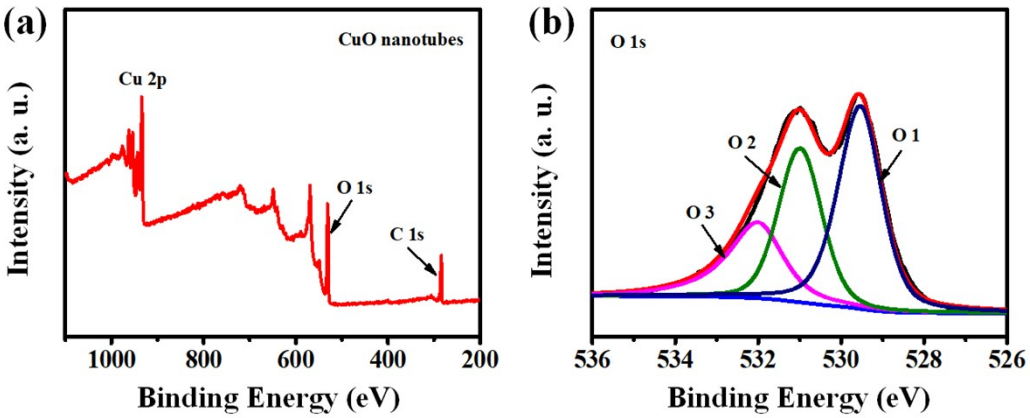

Fig. S3 (a) XPS spectra of the CuO nanotubes. (b) High-resolution XPS spectra of O 1s for CuO nanotubes.

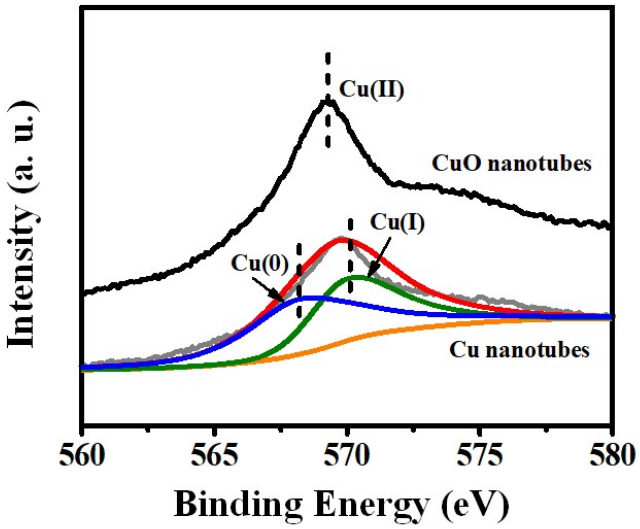

Fig. S4 Cu LMM AES spectra of CuO nanotubes and Cu nanotubes.

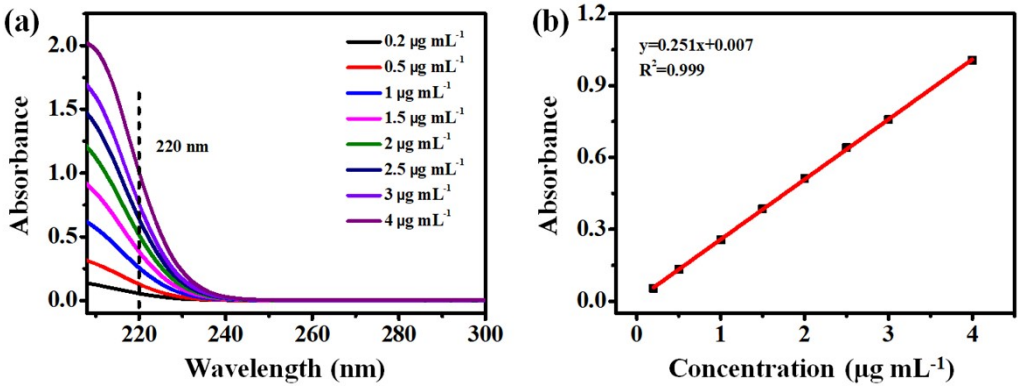

Fig. S5 (a) UV-vis absorption spectroscopy for various concentrations of NO_3^--N. (b) The concentration-absorbance calibration curve of NO_3^--N.

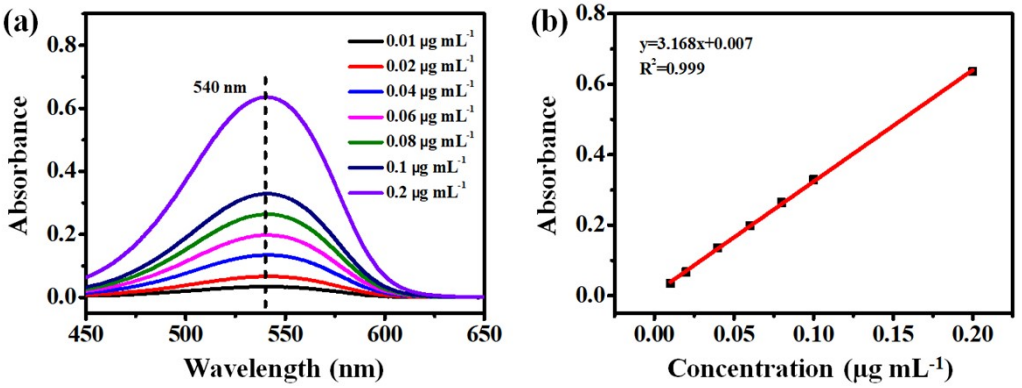

Fig. S6 (a) UV-vis absorption spectroscopy for various concentrations of NO_2^--N. (b) The concentration-absorbance calibration curve of NO_2^--N.

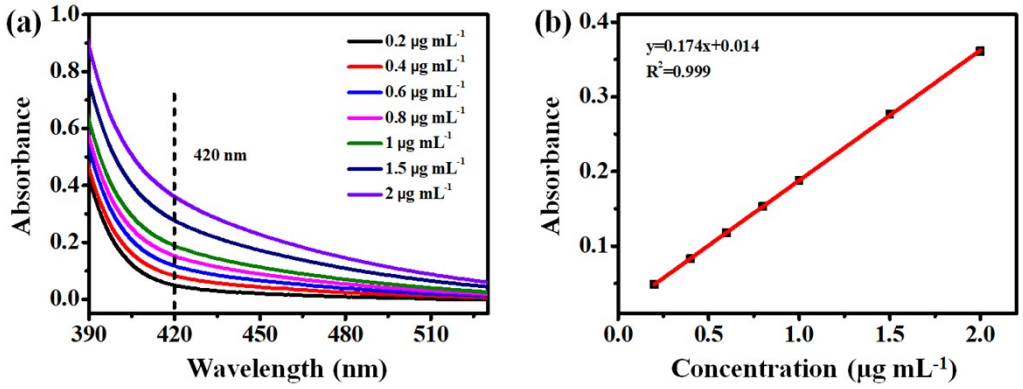

Fig. S7 (a) UV-vis absorption spectroscopy for various concentrations of NH_3-N. (b) The concentration-absorbance calibration curve of NH_3-N.

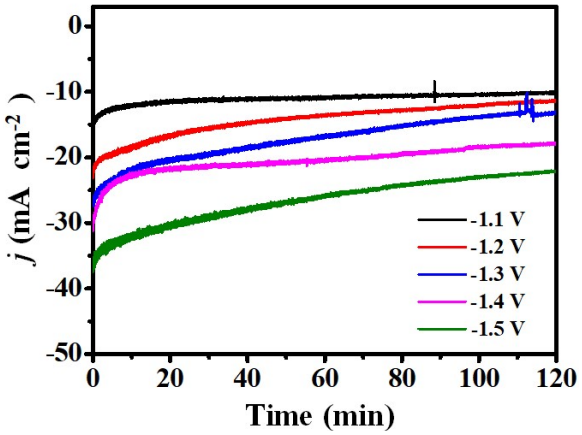

Fig. S8 Chronoamperometric measurements of Cu nanotubes at various potentials in 0.5 M K_2SO_4 solution containing 50 ppm NO_3^--N.

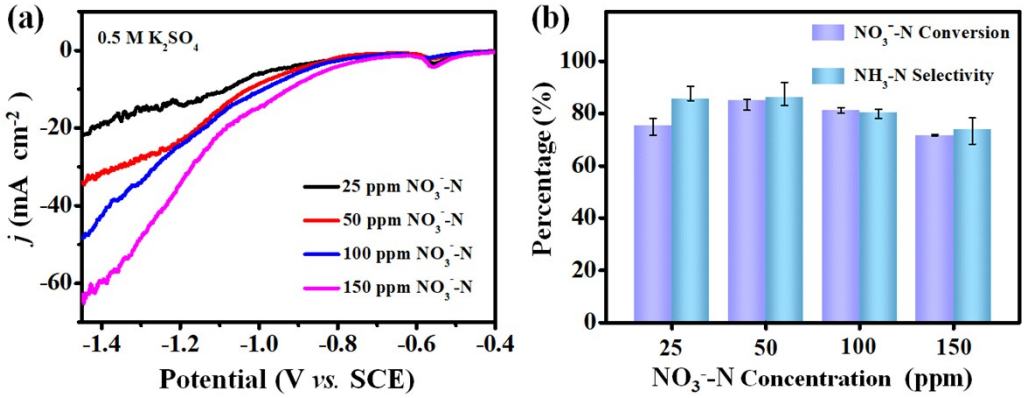

Fig. S9 (a) LSV curves for Cu nanotubes with different concentration of nitrate. (b) The comparisons of NO_3^--N conversion rate and NH_3-N selectivity for Cu nanotubes at different nitrate concentrations.

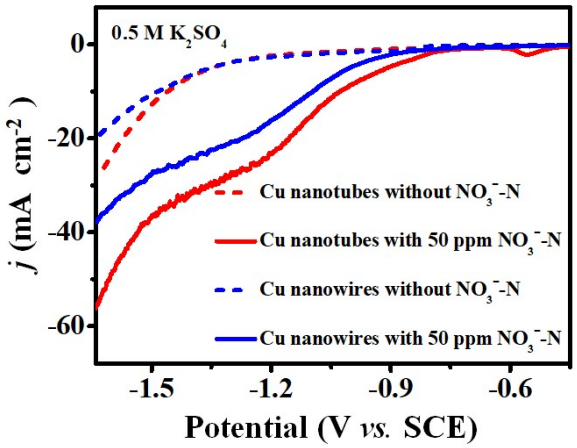

Fig. S10 LSV curves of Cu nanotubes and Cu nanowires.

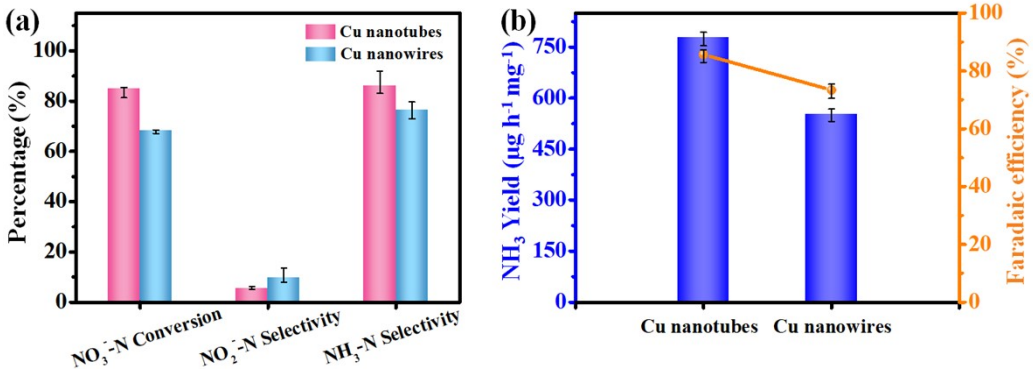

Fig. S11 (a) The comparisons of NO_3^--N conversion rate, NO_2^--N selectivity, and NH_3-N selectivity between Cu nanotubes and Cu nanowires. (b) NH_3 yield rate and Faradaic efficiency of Cu nanotubes and Cu nanowires at -1.3 V *vs*. SCE for 2 h.

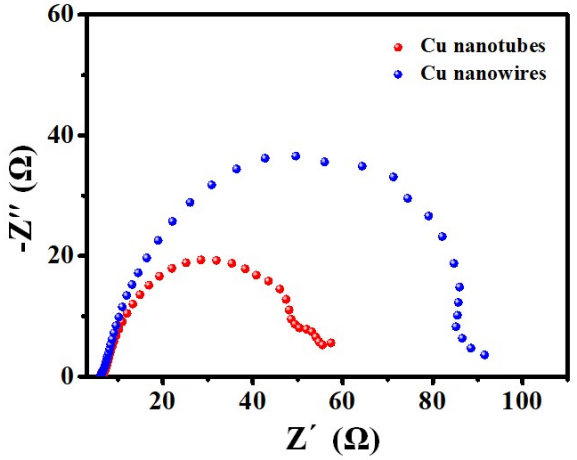

Fig. S12 Nyquist plots for Cu nanotubes and Cu nanowires recorded at -1.2 V (*vs*. SCE) in 0.5 M K_2SO_4 solution. The frequency ranges from 100 kHz to 0.1 Hz.

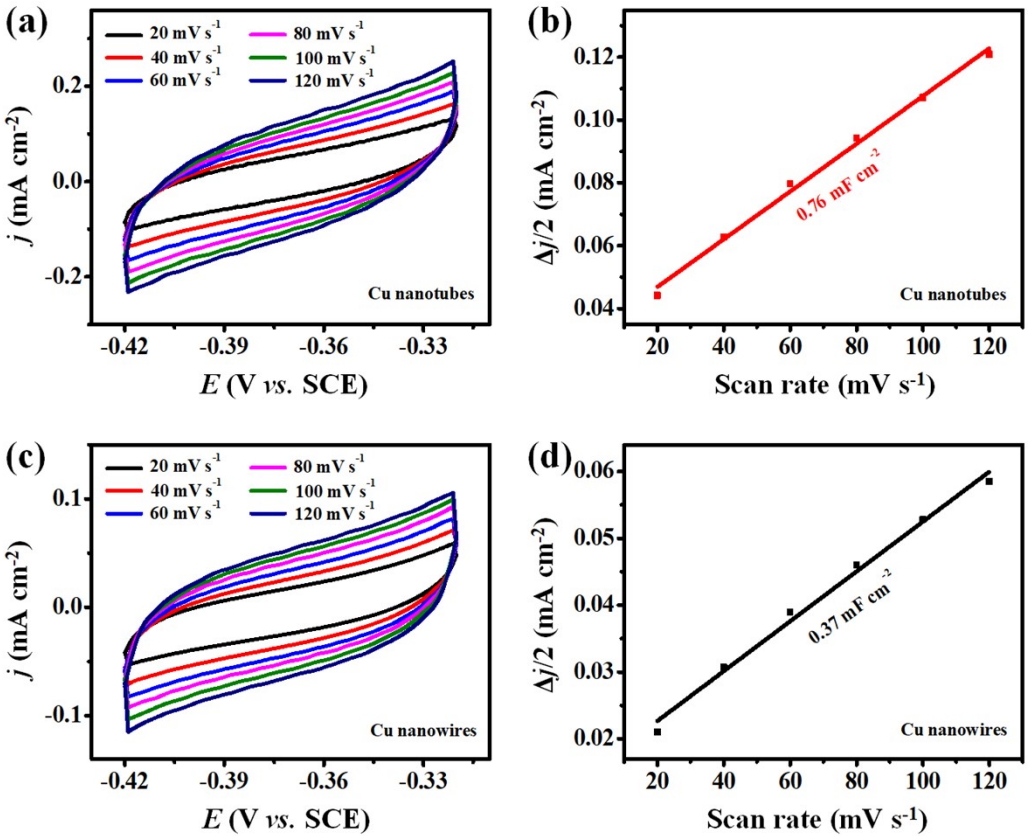

Fig. S13 Cyclic voltammograms for (a) Cu nanotubes and (c) Cu nanowires recorded with various scan rates in 0.5 M K_2SO_4 solution. Capacitive current densities at -0.37 V (*vs*. SCE) derived from CVs against scan rates for (b) Cu nanotubes, and (d) Cu nanowires.

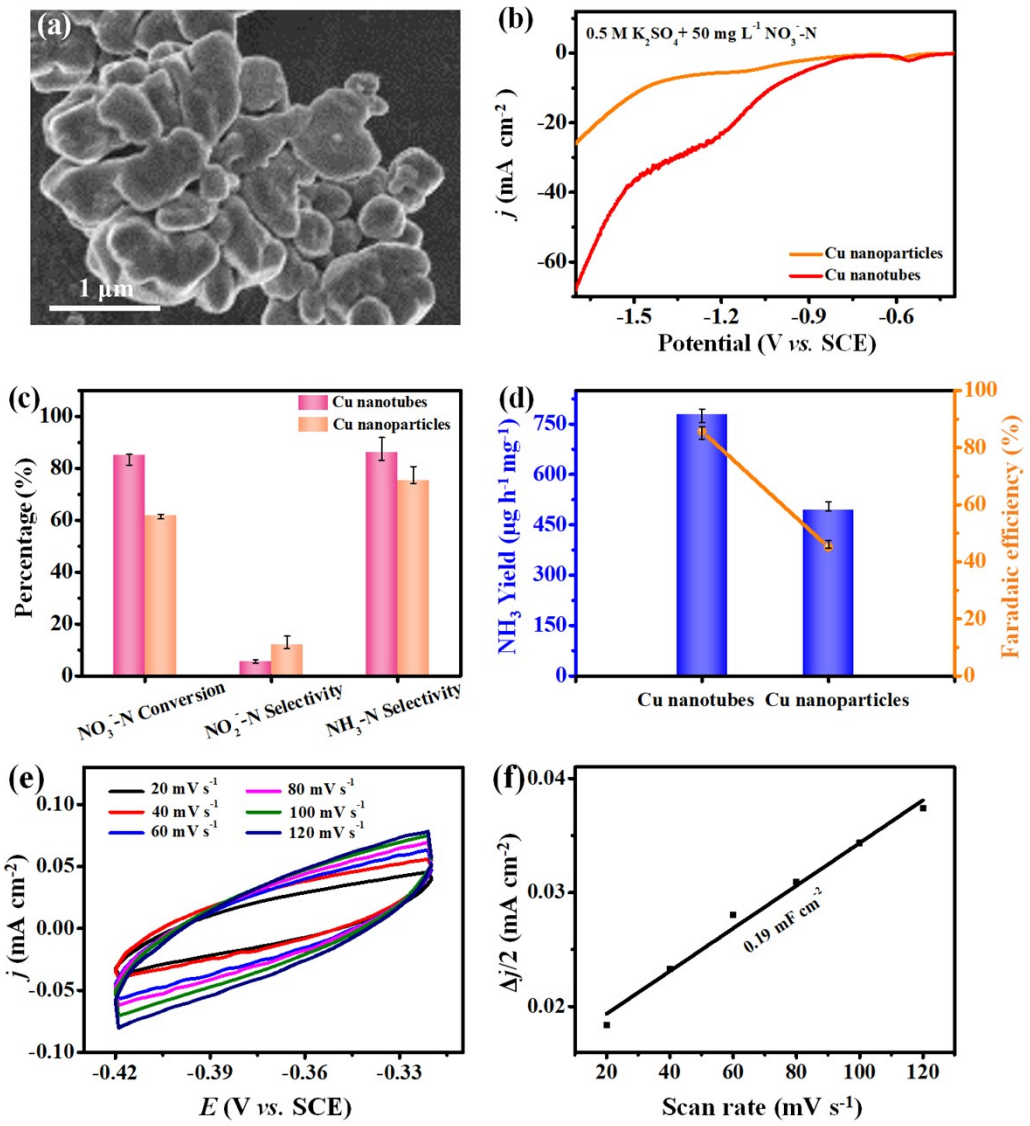

Fig. S14 (a) SEM image for Cu nanoparticles. (b) LSV curves of Cu nanotubes and Cu nanoparticles. (c) The comparisons of NO_3^--N conversion rate, NO_2^--N selectivity, and NH_3-N selectivity between Cu nanotubes and Cu nanoparticles. (d) NH_3 yield rate and Faradaic efficiency of Cu nanotubes and Cu nanoparticles at -1.3 V *vs*. SCE for 2 h. (e) Cyclic voltammograms recorded with various scan rates in 0.5 M K_2SO_4 solution, and (f) capacitive current densities at -0.37 V (*vs*. SCE) derived from CVs against scan rates for Cu nanoparticles.

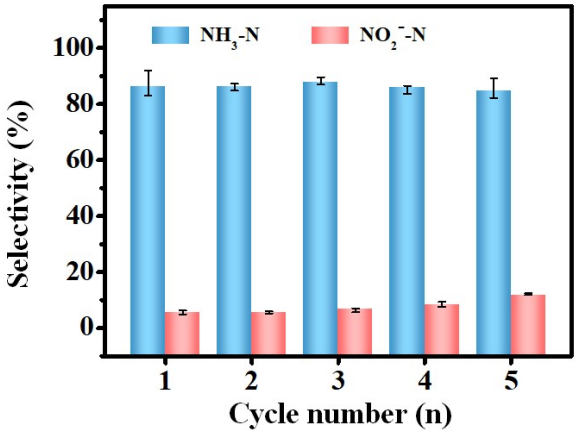

Fig. S15 Selectivity of NH_3-N and NO_2^--N for Cu nanotubes after continuous cycling test at -1.3 V *vs*. SCE.

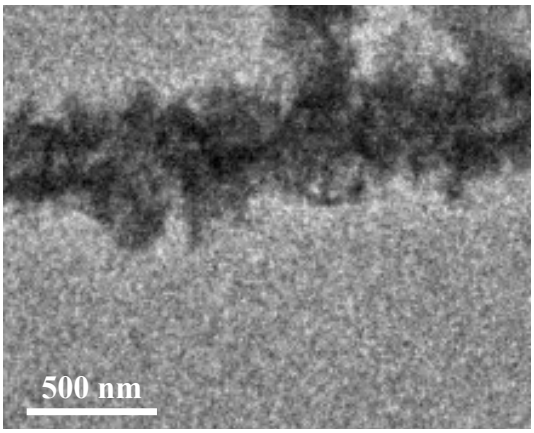

Fig. S16 TEM image of Cu nanotube after stability test.

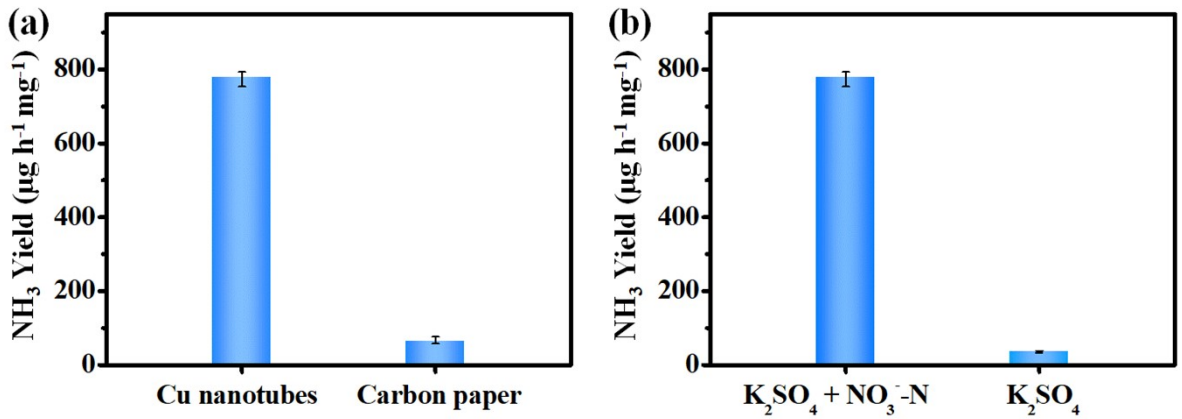

Fig. S17 (a) NH_3 yield rates of the Cu nanotubes and carbon paper at -1.3 V. (b) NH_3 yield rates of the Cu nanotubes in 0.5 M K_2SO_4 solution with and without 50 mg L^{-1} NO_3^--N.

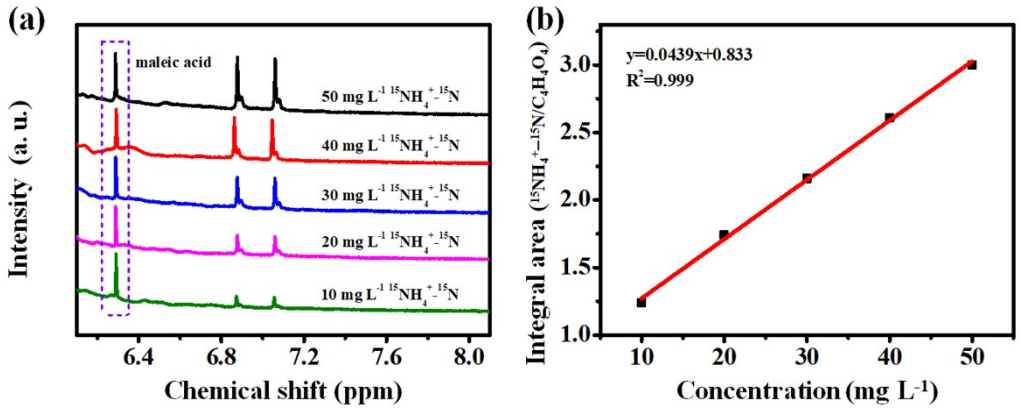

Fig. S18 (a) The ^{1}H NMR spectra of $^{15}NH_4^+$ with different $^{15}NH_4^+$-^{15}N concentration. (b) The standard curve of integral area ($^{15}NH_4^+$-^{15}N / $C_4H_4O_4$) against $^{15}NH_4^+$-^{15}N concentration.

Table S1. Comparisons of the NO_3RR performance for Cu nanotubes with recently reported catalysts.

Catalysts	Electrolyte	Potential	NH_3 yield	FE	NH_3-N selectivity	Ref.
Cu nanotubes	**0.5 M K_2SO_4 + 50 ppm NO_3^--N**	**-1.3 V vs. SCE**	**778.6 μg h^{-1} mg^{-1}**	**85.7%**	**86.2%**	**This work**
Cu nanosheets	0.1 M KOH + 10 mM KNO_3	-0.15 V vs. RHE	390.1 μg h^{-1} $mg_{cat.}^{-1}$	99.7%	--	2
Cu@$Cu_{2+1}O$ NWs	0.5 M K_2SO_4 + 50 ppm NO_3^--N	-1.2 V vs. SCE	576.53 μg h^{-1} $mg_{cat.}^{-1}$	87.07%	76%	3
Cu-PTCDA	0.1 M PBS + 500 ppm KNO_3	-0.4 V vs. RHE	436 ± 85 μg h^{-1} cm^{-2}	85.9%	--	4
Ir nanotubes	0.1 M $HClO_4$ + 1 M $NaNO_3$	0.06 V vs. RHE	921 μg h^{-1} mg_{cat}^{-1}	84.7%	--	5
Cu/GO/Ti	0.05 M Na_2SO_4 + 50 mg/L NO_3^--N	At the current of 0.05 A	--	--	50.37%	6
Cu/rGO/graphite plate	0.02 M NaCl + 0.02 M $NaNO_3$	-1.4 V vs. SCE	--	--	29.93%	7
Cu/Ni composite electrodes	0.1 M Na_2SO_4 + 50 ppm NO_3^--N	At a constant current of 3 mA cm^{-2}	--	--	83.2%	8
$Ag_{27}Ni_{73}$	1 M NaOH + 20 mM $NaNO_3$	-1.3 V vs. SCE	--	--	77.8%	9

References

1. Y. Wang, W. Zhou, R. Jia, Y. Yu and B. Zhang, *Angew. Chem. Int. Ed.*, 2020, **59**, 5350-5354.
2. X. Fu, X. Zhao, X. Hu, K. He, Y. Yu, T. Li, Q. Tu, X. Qian, Q. Yue, M. R. Wasielewski and Y. Kang, *Appl. Mater. Today*, 2020, **19**, 100620.
3. T. Ren, K. Ren, M. Wang, M. Liu, Z. Wang, H. Wang, X. Li, L. Wang and Y. Xu, *Chem. Eng. J.*, 2021, **426**, 130759.
4. G.-F. Chen, Y. Yuan, H. Jiang, S.-Y. Ren, L.-X. Ding, L. Ma, T. Wu, J. Lu and H. Wang, *Nat. Energy*, 2020, **5**, 605-613.
5. J. Y. Zhu, Q. Xue, Y. Y. Xue, Y. Ding, F. M. Li, P. Jin, P. Chen and Y. Chen, *ACS Appl. Mater. Interfaces*, 2020, **12**, 14064-14070.
6. J. Wang, S. Wang, Z. Zhang and C. Wang, *J. Environ. Manage.*, 2020, **276**, 111357.
7. D. Yin, Y. Liu, P. Song, P. Chen, X. Liu, L. Cai and L. Zhang, *Electrochim. Acta*, 2019, **324**, 134846.
8. Y.-J. Shih, Z.-L. Wu, Y.-H. Huang and C.-P. Huang, *Chem. Eng. J.*, 2020, **383**, 123157.
9. L. Mattarozzi, S. Cattarin, N. Comisso, N. El Habra, P. Guerriero, M. Musiani and L. Vázquez-Gómez, *Electrochim. Acta*, 2020, **346**, 136240.